

# DNA-Based Hydrogels with Multidrug Sequential Release for Promoting Diabetic Wound Regeneration

Wei Li,<sup>¶</sup> Hui Xie,<sup>¶</sup> Liping Gou, Ye Zhou, Hao Wang, Ruoqing Li, Yong Zhang, Shuyun Liu, Jingping Liu, Yanrong Lu, Zhengliang Eric He, Nan Chen, Jiang Li, Ying Zhu,<sup>\*</sup> Chengshi Wang,<sup>\*</sup> and Min Lv<sup>\*</sup>



Cite This: *JACS Au* 2023, 3, 2597–2608



Read Online

ACCESS |

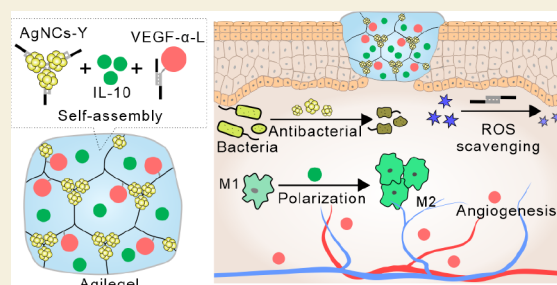
Metrics & More

Article Recommendations

Supporting Information

**ABSTRACT:** Diabetic wound (DW) regeneration is highly challenging due to persistent bacterial infection, excessive production of reactive oxygen species (ROS), prolonged inflammatory response, and insufficient angiogenesis. Ideal management requires the integration and sequential release of bactericidal, antioxidative, anti-inflammatory, and angiogenic agents during DW repair. Here, we develop a DNA-based multidrug hydrogel, termed Agilegel, to promote the efficient healing of DW. Hierarchically structured Agilegel can precisely control the sequential release of vascular endothelial growth factor- $\alpha$  (VEGF- $\alpha$ ), silver nanoclusters (AgNCs), and interleukin-10 (IL-10) through covalent bonds in its primary structure (phosphate backbone), noncovalent bonds in its secondary structure (base pairs), and physical encapsulation in its advanced structure (pores), respectively. We demonstrate that Agilegel can effectively eliminate bacterial infection through AgNCs and mitigate ROS production through DNA scaffolds. Moreover, during the inflammatory phase, Agilegel promotes the polarization of macrophages from pro-inflammatory M1 to anti-inflammatory M2 phenotype using IL-10. Subsequently, Agilegel stimulates cell proliferation, angiogenesis, and extracellular matrix formation through the action of VEGF- $\alpha$ , thereby accelerating the closure of DW. Our results indicate that DNA hydrogels confer the capacity to regulate the sequential release of drugs, enabling them to effectively manage the phased intervention of multiple drugs in the treatment of complex diseases within physiological environments.

**KEYWORDS:** diabetic wound regeneration, DNA hydrogel, multidrug sequential release, silver nanoclusters, phased intervention



## INTRODUCTION

Diabetic wound (DW) regeneration is a complex physiological process that involves four sequential yet overlapping phases: hemostasis, inflammation, proliferation, and remodeling.<sup>1</sup> This healing process is often compromised by persistent microbial infection, excessive reactive oxygen species (ROS), prolonged inflammatory response, and insufficient angiogenesis.<sup>2–4</sup> Diabetic individuals are particularly susceptible to bacterial infections due to weakened immune systems, leading to increased morbidity and mortality.<sup>5</sup> Moreover, treating bacterial infections in DWs is challenging due to antimicrobial resistance, and these infections further worsen wound inflammation and oxidative stress.<sup>6</sup> Persistent inflammatory responses greatly hinder the remodeling of the extracellular matrix, maturation of blood vessels, and differentiation of cells.<sup>7,8</sup> Excessive ROS impairs angiogenesis and causes dysfunction in the endothelial cells.<sup>9</sup> Insufficient angiogenesis reduces the blood supply and nutrient availability at the wound site, significantly delaying the healing process.<sup>10</sup> Therefore, there is an urgent need for a multidrug system that can effectively manage DWs through integrated approaches.

Recently, multifunctional hydrogels have emerged as promising candidates for local drug delivery in DW healing

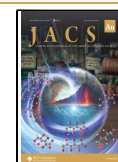
due to their unique properties, including high carrying capacity, desired softness, biodegradability, and high-water content.<sup>11–14</sup> For instance, antibacterial polypeptide hydrogels have been developed to codeliver MnO<sub>2</sub> nanosheets and insulin for the treatment of DWs infected with multidrug-resistant bacteria.<sup>15</sup> Additionally, poly(vinyl alcohol) hydrogels with ROS-scavenging properties have been utilized to codeliver mupirocin and granulocyte-macrophage colony-stimulating factor to promote the regeneration of DWs.<sup>6</sup> However, conventional hydrogels often cannot sequentially release multiple drugs at different phases of the wound-healing process. Simultaneous or random release of drugs can lead to reduced utilization and efficacy of therapeutic agents, which do not meet the requirement for phased intervention with multiple drugs. Therefore, an ideal and versatile hydrogel for DWs should possess a well-coordinated integration of

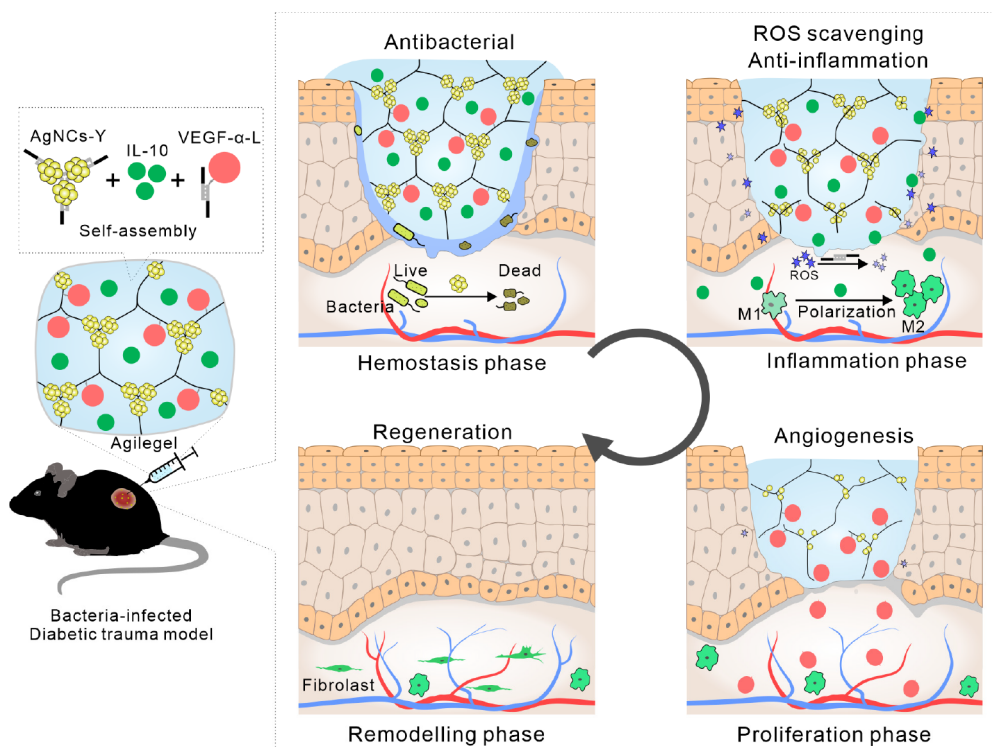
Received: July 26, 2023

Revised: August 22, 2023

Accepted: August 22, 2023

Published: August 29, 2023



Scheme 1. Agilegel Promotes Diabetic Wound Regeneration<sup>a</sup>

<sup>a</sup>Agilegel is assembled with DNA monomers and incorporates VEGF- $\alpha$ , AgNCs, and IL-10. Hierarchical Agilegel releases VEGF- $\alpha$ , AgNCs, and IL-10 sequentially through covalent bonds, noncovalent bonds, and physical encapsulation. Three drugs play their respective roles in different stages of sterilization, anti-inflammation, ROS scavenging, and angiogenesis promotion.

antibacterial, antioxidant, anti-inflammatory, and angiogenic agents with the ability to sequentially release these agents during the wound repair process.

DNA hydrogels, as hierarchical self-assembling biological materials, not only possess common features shared by other hydrogels, but also exhibit designable microstructures and tunable macroscopic mechanical, chemical, and biological properties.<sup>16–18</sup> With their modifiability, biodegradability, and biocompatibility, DNA hydrogels serve as excellent carriers for the localized release of complex drugs.<sup>19,20</sup> They have found extensive applications in the treatment of various conditions, including spinal cord injuries,<sup>21</sup> cancer,<sup>22,23</sup> arthritis,<sup>24,25</sup> alveolar bone,<sup>26</sup> and wound healing.<sup>27</sup> Hierarchically structured DNA-based hydrogels enable the utilization of covalent modifications on the primary structure (phosphate backbone) or noncovalent interactions on the secondary structure (base pairs) for drug delivery. Moreover, their advanced structure, such as pores, allows for the encapsulation of cargo. These diverse physiochemical forces within DNA hydrogels offer the potential for the sequential release of different therapeutic agents. Additionally, DNA molecules have been employed as effective scavengers of ROS due to their sensitivity to various ROS species.<sup>28</sup> This property enables DNA hydrogels to alleviate oxidative stress in DWs. However, there have been no reports on the sequential release of multiple drugs using DNA hydrogels for the phased intervention in DW repair. In this study, we have developed a DNA-based multidrug sequential-release hydrogel, termed Agilegel, for the controlled delivery of interleukin 10 (IL-10), silver nanoclusters (AgNCs), and vascular endothelial growth

factor- $\alpha$  (VEGF- $\alpha$ ) to promote the regeneration of diabetic wound (Scheme 1).

## RESULTS AND DISCUSSION

### Design of Agilegel

We design a DNA-based and multidrug sequential-release hydrogel, termed Agilegel, which integrates IL-10, AgNCs, and VEGF- $\alpha$  for antibacterial, ROS scavenging, anti-inflammation, and angiogenesis promotion. Agilegel is a 3D physically cross-linked DNA hydrogel composed of two DNA dendritic monomers, Y and L. Hierarchically structured DNA hydrogels provide three types of drug loading *via* covalent binding to DNA phosphate backbones, noncovalent binding to base pairs, and physical encapsulation of the advanced porous structure. Different physiochemical forces confer the ability to release drugs from Agilegel sequentially.<sup>29–31</sup> The drugs integrated into Agilegel here include the following: (1) AgNCs, as antibacterial agents, have proved to have superior antibacterial properties due to their ultrasmall size and highly efficient nanoreservoirs of Ag atoms.<sup>32,33</sup> Compared to Ag ions, AgNCs can sustainably release Ag atoms and avoid the Ag ion pulse, which can significantly reduce their *in vivo* cytotoxicity.<sup>34,35</sup> AgNCs are synthesized *in situ* by using the cytosine-rich Y-shaped DNA monomer as a template. The programmable DNA template can precisely control the spatial structure of AgNCs and prevent them from aggregating, which enables AgNCs to maintain their antibacterial activity for much longer than Ag nanoparticles.<sup>36</sup> (2) IL-10, one of the most potent immune modulators, activates the transition of macrophages from pro-inflammatory M1 to anti-inflammatory M2 phenotype,<sup>37–39</sup> which is encapsulated in Agilegel's pores and plays

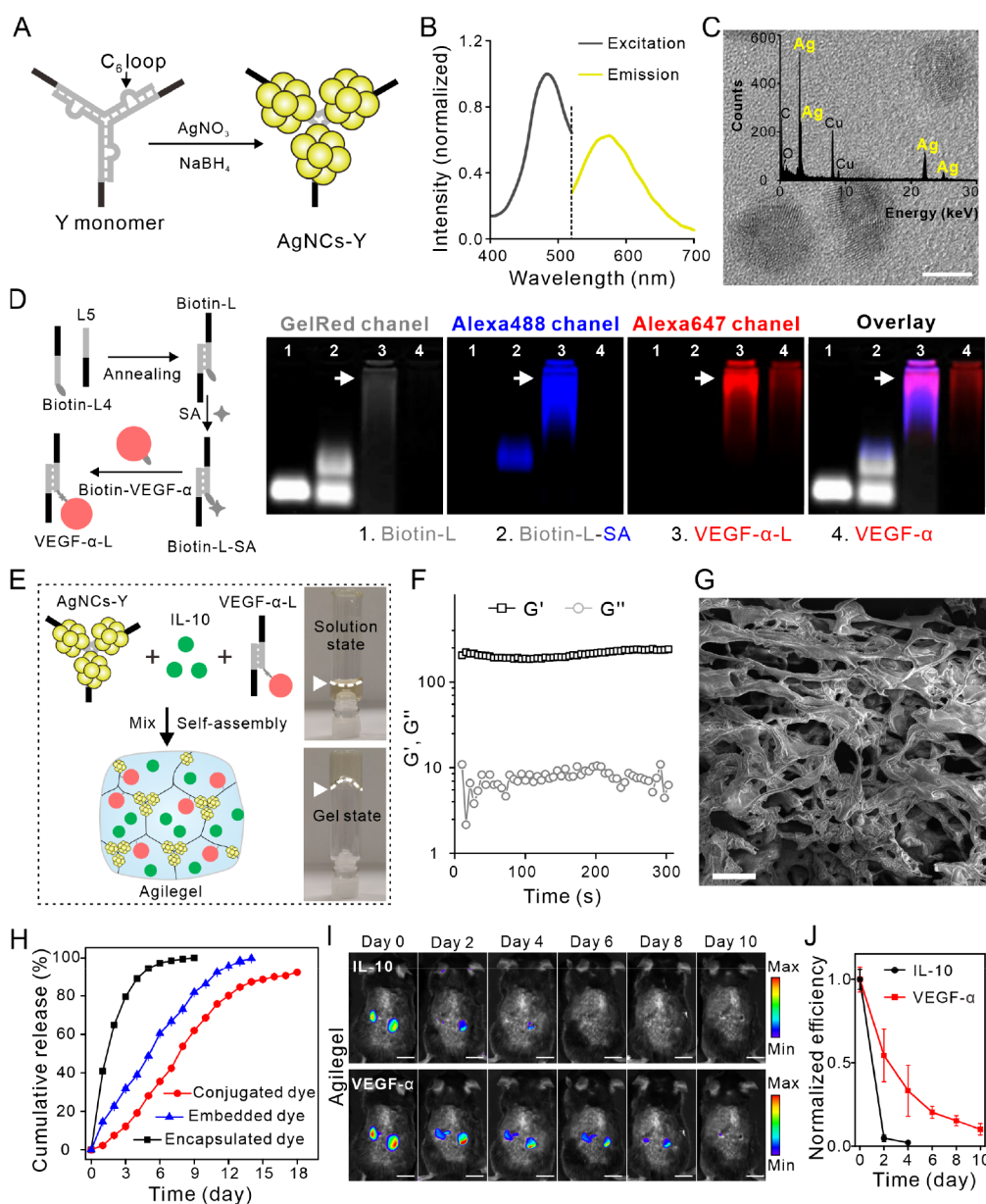


**Figure 1.** Synthesis and characterization of Agilegel. (A) Schematic illustration of AgNCs-Y synthesis. (B) Excitation and emission spectra of AgNCs-Y nanostructure (ex: 473 nm, em: 565 nm). (C) TEM image of AgNCs-Y nanostructure, scale bar = 5 nm. Inset: Elemental analysis of AgNCs-Y nanostructure by EDS. (D) Conjugation of the L monomer with VEGF- $\alpha$  through the biotin-SA interaction. SA was labeled with Alexa488 and VEGF- $\alpha$  was labeled with Alexa647. Lane 1: Biotin-L, lane 2: Biotin-L-SA, lane 3: VEGF- $\alpha$ -L, lane 4: VEGF- $\alpha$ . (E) Schematic diagram of Agilegel preparation and photographs of Agilegel in the solution and gel states. (F) Rheological analysis of Agilegel, scale bar = 100  $\mu$ m. (G) SEM image of Agilegel, scale bar = 100  $\mu$ m. (H) Release kinetics of different dyes by the DNA hydrogel. (I, J) *In vivo* release of IL-10 and VEGF- $\alpha$  in Agilegel. Optical imaging (I) and fluorescence quantification (J) of Alexa488-labeled IL-10 and Alexa647-labeled VEGF- $\alpha$ , scale bar = 10 mm (IL-10, max:  $6 \times 10^9$ , min:  $0.5 \times 10^9$ . VEGF- $\alpha$ , max:  $4.5 \times 10^9$ , min:  $0.5 \times 10^9$ ).

an anti-inflammatory role. (3) VEGF- $\alpha$  is covalently conjugated to the L DNA monomer through the strong interaction of biotin-streptavidin (SA), which is used to improve vascular development and promote angiogenesis.<sup>40,41</sup> In addition, DNA structures themselves are sensitive to various ROS and serve as effective ROS scavengers.<sup>27</sup>

### Construction and Characterization of Agilegel

To synthesize Agilegel, we constructed two building blocks: AgNCs-Y and VEGF- $\alpha$ -L. AgNCs have been fabricated in previous work using DNA scaffolds with a six-base cytosine loop ( $C_6$  loop).<sup>42</sup> The Y-shaped DNA scaffold (Y monomers), containing 3  $C_6$  loops, was prepared by annealing three single-

stranded DNA (ssDNA) strands with rationally designed sequences (Figure S1 and Table S1), and its successful formation was confirmed by polyacrylamide gel electrophoresis (PAGE, Figure S2). AgNO<sub>3</sub> was then added to the Y monomer solution and reduced with NaBH<sub>4</sub> to produce the AgNCs-Y nanostructure (Figure 1A). As shown in Figure 1B, AgNCs-Y exhibited a characteristic yellow fluorescence, which is a typical property of noble metal nanoclusters. Furthermore, agarose gel electrophoresis (AGE) showed that the AgNCs could be tightly embedded within the Y monomer (Figure S3). Transmission electron microscopy (TEM) revealed that the AgNCs-Y nanostructure exhibited a dispersed typical nano-

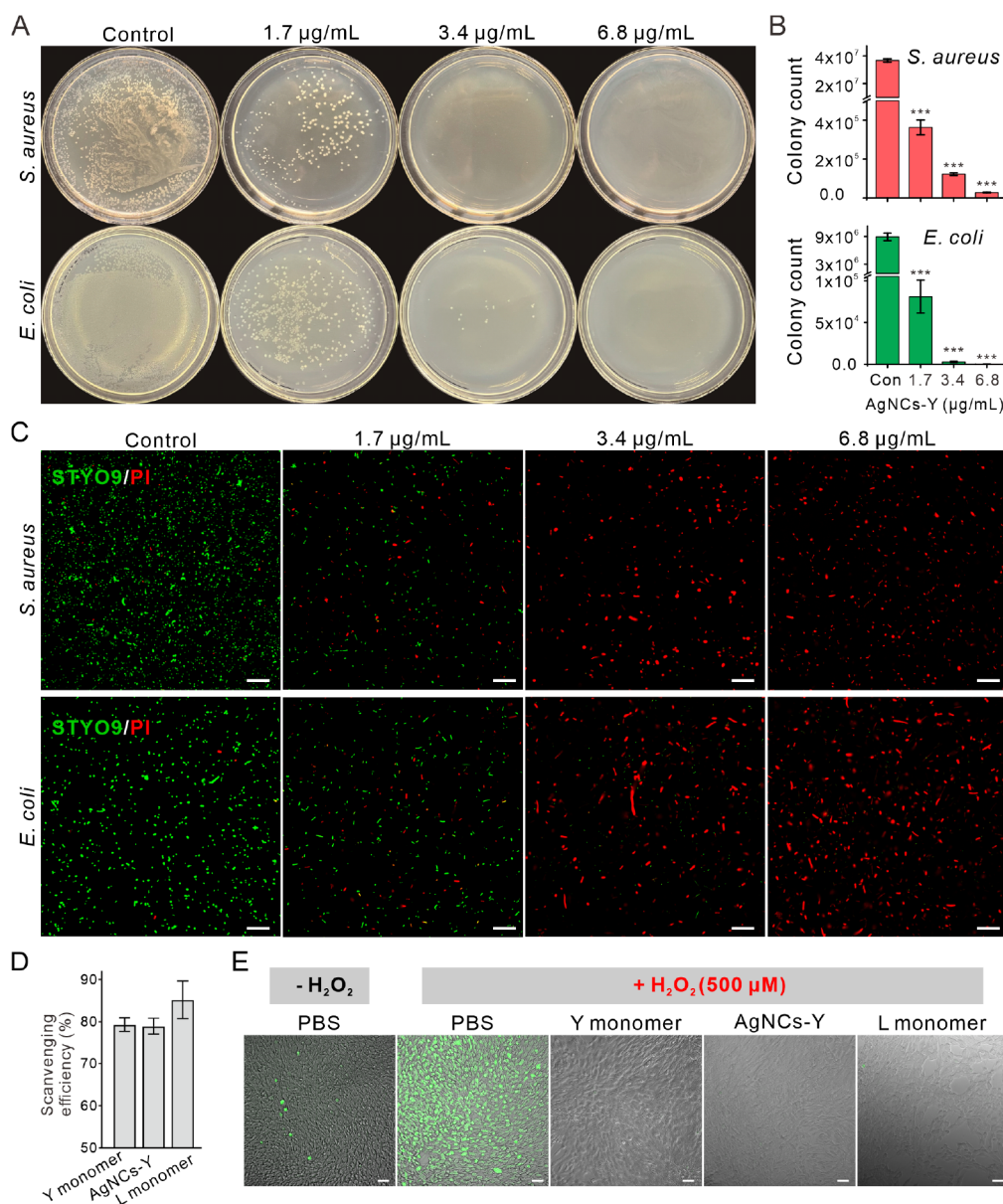


**Figure 2.** AgNCs-Y combats bacteria and scavenges ROS *in vitro*. (A) Bacterial colony images and (B) number after treatment with AgNCs-Y for 4 h at 37 °C. \*\*\* $P < 0.001$  vs control. (C) Confocal images of live and dead *S. aureus* and *E. coli* after treatment with AgNCs-Y. PBS as a control, scale bar = 20  $\mu\text{m}$ . (D)  $\bullet\text{OH}$ -scavenging efficiency of the Y monomer, AgNCs-Y, and the L monomer. (E) ROS detection in HaCaT cells after incubation with the Y monomer, AgNCs-Y, and the L monomer, scale bar = 50  $\mu\text{m}$ .

cluster structure with an average diameter of 6.3 nm (Figure 1C). The elemental analysis of the nanoclusters by energy dispersive spectrometry (EDS) showed that silver was the major element present, providing strong evidence for the successful formation of the AgNCs-Y nanostructure.

To obtain VEGF- $\alpha$ -L, both VEGF- $\alpha$  and L DNA monomers were first modified with biotin. They were then covalently linked via strong biotin–streptavidin (SA) interaction. AGE showed that the L-shaped DNA monomer, and VEGF- $\alpha$  overlapped well (Figure 1D), indicating that VEGF- $\alpha$  was successfully conjugated to the L monomer to form VEGF- $\alpha$ -L. Next, IL-10 was premixed with AgNCs-Y and VEGF- $\alpha$ -L respectively, and these two mixtures were incubated at room temperature to self-assemble into Agilegel, where the solution state of the mixture immediately converted to the gel state (Figure 1E). Rheological analysis showed that the shear-

storage modulus ( $G'$ ) of Agilegel was higher than its shear-loss modulus ( $G''$ ) (Figure 1F), a typical feature of the gel-like state. In addition, scanning electron microscopy (SEM) revealed clear porous microstructures within Agilegel (Figure 1G), suggesting hydrogel formation with the ability to encapsulate IL-10.

Subsequently, we evaluated the sequential release of different Agilegels loaded *in vitro* and *in vivo*. As the fluorescence signal from AgNCs was difficult to detect at our working concentration, SYTO 60 was embedded in the DNA backbone (embedded dye) to mimic the AgNCs-DNA interaction. Cy3 was covalently conjugated to the L-shaped DNA monomer (conjugated dye), and Alexa488 was encapsulated in the holes of the DNA hydrogel (encapsulated dye). As shown in Figure 1H, three fluorescent dyes exhibited different release dynamics, with the encapsulated dye releasing

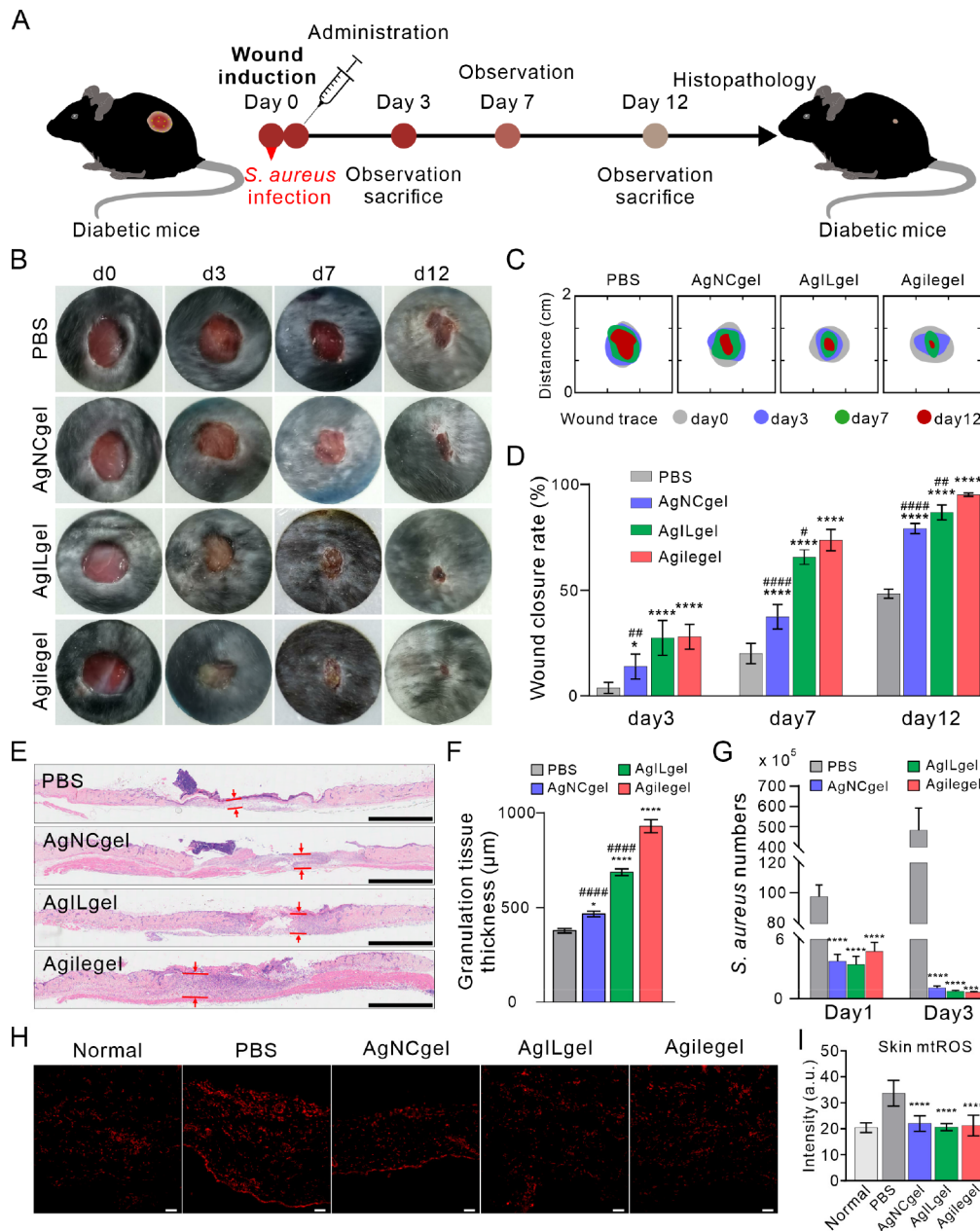


**Figure 3.** Agilegel promotes diabetic wound healing. (A) Scheme of bacterial infection and subsequent treatment in the diabetic mouse model. (B) Representative photos of wounds on days 0, 3, 7, and 12 after wounding. (C) Wound closure traces of the indicated groups. (D) Quantification of the DW closure rate after wounding ( $n = 6$ ). (E) H&E-stained images of dermal tissue on day 12 after different treatment. The red line denotes the thickness of dermal tissues, scale bar = 2 mm. (F) Quantification of dermal thickness in each group on day 12 after wounding. (G) The number of *S. aureus* colonies from wounds. Fluorescence images (H) and intensity (I) of MitoSOX in skin tissues, scale bar = 50  $\mu\text{m}$ . \* $P < 0.05$ , \*\* $P < 0.01$ , \*\*\* $P < 0.001$ , \*\*\*\* $P < 0.0001$  vs PBS. # $P < 0.05$ , ## $P < 0.01$ , ### $P < 0.001$ , #### $P < 0.0001$  vs Agilegel.

the fastest, followed by the embedded dye, and finally the conjugated dye. Nearly 80% of the encapsulated dye was released in just 3 days. The same percentages of the embedded and conjugated dyes were released in 8 and 12 days, respectively. To verify the release capability of Agilegel *in vivo*, we injected Agilegel into the wound bed of diabetic mice locally and monitored the fluorescence signal of IL-10 and VEGF- $\alpha$  at different time points. The mixture of IL-10 and VEGF- $\alpha$  was used as a control. As shown in Figure 1I and J, the signal of IL-10 decreased rapidly but persisted for 4 days. However, the VEGF- $\alpha$  signal decreased more slowly and was still present in the wounds at least 10 days after injection. No detectable signal of either IL-10 or VEGF- $\alpha$  was observed in

mice after 1 day of treatment (Figure S4). These results confirm our design and demonstrate the sequential release of multiple drugs in the DNA hydrogel through its hierarchical structure, which has great potential for DW regeneration.

#### AgNCs-Y Combats Bacteria and Scavenges ROS *In Vitro*

Controlling bacterial infection is crucial for wound healing in diabetics. To confirm the antibacterial properties of Agilegel, we initially assessed the effectiveness of AgNCs-Y in combating *Staphylococcus aureus* (*S. aureus*, Gram-positive) and *Escherichia coli* (*E. coli*, Gram-negative) *in vitro* using the plate count method. The result showed that 6.8  $\mu\text{g}/\text{mL}$  AgNCs-Y could effectively inhibit the growth of both *S. aureus* and *E. coli*

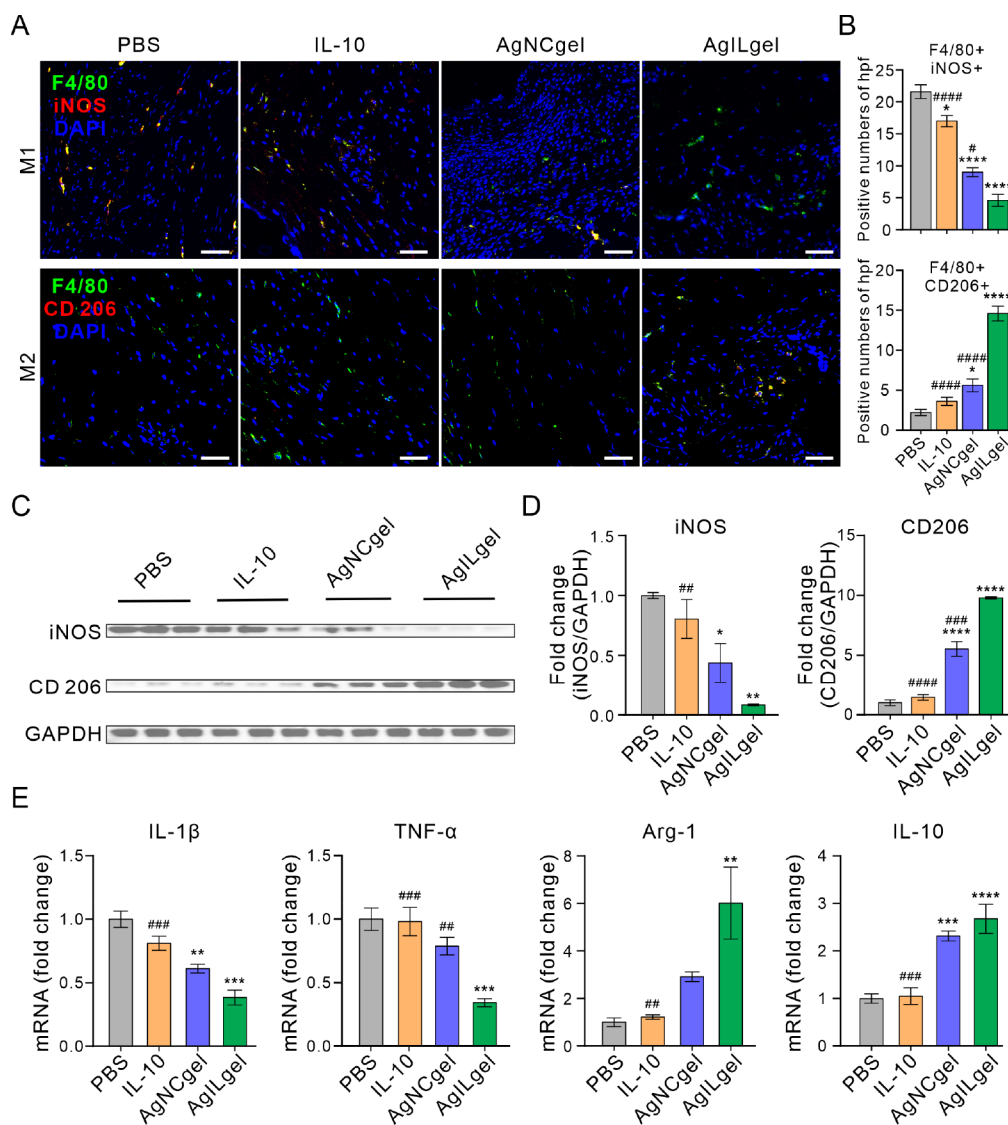


**Figure 4.** Sequential release of IL-10 attenuates the inflammatory response in DWs. (A) IF staining of Macrophages in the skins at 3 days post-treatment, scale bar = 50  $\mu$ m. (B) Quantification of F4/80+iNOS+ M1 and F4/80+CD206+ M2 cells. (C, D) WB and quantification analysis of skin tissue iNOS and CD206 protein levels at day 3 after treatment. (E) qRT-PCR analysis of skin tissue IL-1 $\beta$ , TNF- $\alpha$ , Arg-1, and IL-10 mRNA levels at day 3 after treatment. \* $P$  < 0.05, \*\* $P$  < 0.01, \*\*\* $P$  < 0.001, \*\*\*\* $P$  < 0.0001 vs PBS. # $P$  < 0.05, ## $P$  < 0.01, ### $P$  < 0.001, #### $P$  < 0.0001 vs AgILgel.

(Figure 2A and B). Furthermore, compared to the normal bacteria, the two types of bacterial cells exhibited morphological destruction and membrane damage in the presence of AgNCs-Y (Figures 2C and S5), which aligns with the typical antimicrobial action of AgNCs. These findings suggest that AgNCs-Y is effective in fighting against bacteria. Importantly, AgNCs-Y presented minimal cytotoxicity (Figure S6) and *in vivo* nontoxic biodegradability (Figure S7), showing good biocompatibility.

Under diabetic conditions, immune cells can generate excessive ROS, which impedes wound healing. It has been reported that scavenging excess ROS promotes the regeneration of DWs.<sup>6,27</sup> DNA molecules are sensitive to a variety of ROS radicals and possess scavenging capabilities.<sup>43,44</sup> To verify this, we used methylene blue (MB) as a hydroxyl radical ( $\bullet$ OH) indicator to test the ROS-scavenging activity of DNA. Hydroxyl radicals were generated by the Fenton reaction and then incubated with the Y monomer, AgNCs-Y, and the L

monomer for 30 min each. Finally, MB was added to each group and incubated for 2 h. MB was almost completely consumed in the control group, while Y monomer, AgNCs-Y and L monomer can maintain at least 80% of MB, indicating the Y monomer, AgNCs-Y, and the L monomer can effectively scavenge hydroxyl radicals (Figure 2D and Figure S8). The intracellular ROS-scavenging properties of DNA nanostructures were also investigated. Human epidermal keratinocyte (HaCaT) cells were incubated with 500  $\mu$ M H<sub>2</sub>O<sub>2</sub> overnight to produce intracellular ROS, followed by incubation with the Y monomer, AgNCs-Y, and the L monomer. 2',7'-Dichlorodihydrofluorescein diacetate (DCFH-DA) was used as the intracellular ROS indicator. We found that the fluorescence signal in the Y monomer, AgNCs-Y, and L monomer groups was significantly lower than that in the PBS group (Figure 2E), indicating the efficient scavenging of intracellular ROS by DNA-based nanostructures.

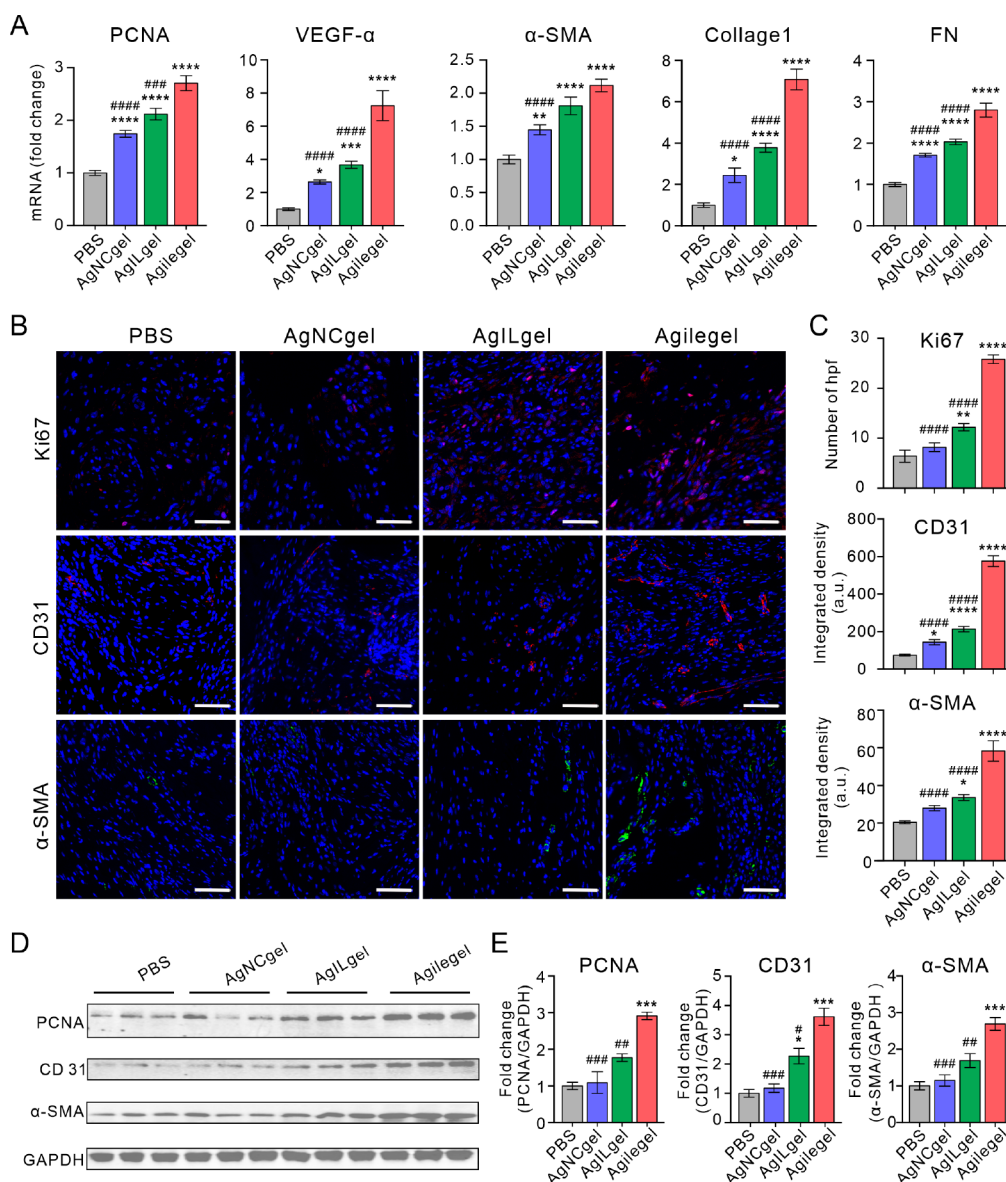


**Figure 5.** Prolonged retention of VEGF- $\alpha$  facilitates proliferation, angiogenesis, and extracellular matrix formation in wound tissue. (A) qRT-PCR analysis of skin tissue PCNA, VEGF- $\alpha$ ,  $\alpha$ -SMA, collagen1, and FN mRNA levels on day12 after treatment. (B, C) IF staining and quantification of skin tissue Ki67, CD31, and  $\alpha$ -SMA on day12 after treatment, scale bar = 50  $\mu$ m. (D, E) WB and quantification analysis of skin tissue PCNA, CD31, and  $\alpha$ -SMA protein levels at day 12 after treatment. \* $P$  < 0.05, \*\* $P$  < 0.01, \*\*\* $P$  < 0.001, \*\*\*\* $P$  < 0.0001 vs PBS. # $P$  < 0.05, ## $P$  < 0.01, ### $P$  < 0.001, #### $P$  < 0.0001 vs Agilegel.

### Agilegel Promotes Diabetic Wound Healing

The above results suggest that the components of Agilegel have efficient bactericidal and ROS scavenging abilities *in vitro*. Next, to determine whether Agilegel could accelerate DW regeneration *in vivo*, we created wounds in a diabetic mouse model and evaluated the therapeutic effects of Agilegel. Diabetic mice with *S. aureus*-infected cutaneous wounds were treated with PBS, AgNCgel (only AgNCs integrated within the DNA hydrogel), AgILgel (encapsulated IL-10 based on AgNCgel), or Agilegel. The infected wounds of different groups were photographed on days 0, 3, 7, and 12 (Figure 3A). As shown in Figure 3B–D, on day 3, the infected wounds treated with AgNCgel, Ag ILgel, and Agilegel were much smaller than those in the PBS group, which should be attributed to the antibacterial effect of DNA-templated AgNCs. Infected wounds in both AgILgel and Agilegel groups also

showed significantly less swelling compared to that in the AgNCgel group, suggesting that the anti-inflammatory effect of IL-10 may be effective in promoting wound healing during the inflammation phase. On days 7 and 12, Agilegel improved the closure of infected wounds compared to the AgILgel group, recovering by approximately 73.8% (day 7) and 95.2% (day 12). Once the inflammation has been reduced, the VEGF- $\alpha$  released in Agilegel may promote angiogenesis in the wounds, resulting in the acceleration of tissue regeneration. H&E staining revealed a notable difference in the thickness of the epidermis observed on day 12 for all groups. The dermal thicknesses in the AgNCgel, AgILgel, and Agilegel groups were significantly greater larger than that of in the PBS group. And the wound was almost closed in the Agilegel group (Figure 3E, F). Taken together, these results demonstrate that Agilegel can effectively promote DW regeneration *in vivo*.

To elucidate the mechanism of accelerated DW repair, we comprehensively evaluated the effects of Agilegel on biological and molecular events in four sequential phases of the wound healing process. First, the *in vivo* antibacterial effects were investigated. We collected and cultured *S. aureus* from the wound site on days 1 and day 3. As shown in Figure 3G, the number of viable *S. aureus* colonies in the presence of AgNCgel, AgILgel, or Agilegel was obviously decreased compared to the PBS group. The gradual reduction of *S. aureus* in these groups over time suggested that the AgNCs-integrated hydrogel could effectively inhibit the growth of *S. aureus* in DW beds. Next, we investigate ROS levels *in vivo*. Fresh skin tissue was collected on day 3 and stained with MitoSOX which is an indicator of oxidative stress in tissues or cells. As shown in Figure 3H and I, the fluorescence in the AgNCgel, AgILgel, and Agilegel treatment groups was much lower than that in the PBS group. There was also no significant difference between the AgNCgel, AgILgel, and Agilegel treatment groups and the normal group, indicating that the DNA-based hydrogel is effective in attenuating oxidative stress *in vivo*.

### Sequential Release of IL-10 Attenuates the Inflammatory Response in DWs

An anti-inflammatory microenvironment is beneficial for the transition from the inflammatory phase to the proliferative phase of wound healing, thereby accelerating the process of tissue regeneration. Given the immune-modulating and anti-inflammatory properties of IL-10, we investigated its effects on macrophages and inflammation *in vivo* when it was encapsulated in the DNA hydrogel. We locally injected PBS, free IL-10, AgNCgel, and AgILgel (encapsulated IL-10 based on AgNCgel) into DWs infected with *S. aureus*. On day 3 after wound induction, tissues around the wound sites were collected for immunofluorescence (IF) staining, Western blot (WB), and qRT-PCR analysis. The F4/80 and inducible nitric oxide synthase (iNOS) double-positive signal (F4/80+iNOS+), representing pro-inflammatory M1 macrophages, was significantly lower in the AgILgel group than in the other groups, while the F4/80 and CD206 double-positive (F4/80+CD206+) signal, representing anti-inflammatory M2 macrophages, was much higher (Figure 4A and B), suggesting that AgILgel treatment could significantly decrease the expansion of M1 macrophages while increasing the expansion of M2 macrophages. The same result was confirmed by the WB (Figure 4C and D). There was no significant difference between the PBS and free IL-10-treated groups. This may be because free IL-10 quickly drained off and cannot remain on the wound bed. AgNCgel also significantly decreased M1 and increased M2 compared to the IL-10 and PBS group, which may be attributed to AgNCgel's antibacterial and antioxidant effects derived from AgNCs and DNA scaffolds. qRT-PCR analysis revealed that AgILgel significantly suppressed the expression of pro-inflammatory factors such as interleukin 1 beta (IL-1 $\beta$ ) and tumor necrosis factor alpha (TNF- $\alpha$ ) while inducing the expression of anti-inflammatory factors such as arginase (Arg-1) and IL-10 compared to the IL-10 or PBS group (Figure 4E). Taken together, these data suggest that the sequential release of IL-10 in AgILgel effectively promotes M2 polarization and eliminates inflammatory responses *in vivo*.

### Prolonged Retention of VEGF- $\alpha$ Facilitates Proliferation, Angiogenesis, and Extracellular Matrix Formation in Wound Tissues

After the inflammatory phase, the wound enters the proliferative phase, which includes cell proliferation, angiogenesis, and extracellular matrix formation. VEGF- $\alpha$  is one of the key growth factors for regulating vascular development. We collected wound skin samples from different groups on day 12 after treatment and used qRT-PCR, IF staining, and WB to examine proliferation, angiogenesis, and extracellular matrix (ECM) formation. As shown in Figure 5A, qRT-PCR analysis revealed that the gene expression levels of proliferating cell nuclear antigen (PCNA), angiogenesis-related cytokine VEGF- $\alpha$ ,  $\alpha$ -smooth muscle actin ( $\alpha$ -SMA), ECM formation-related collagen1, and fibronectin (FN) were significantly increased in the AgNCgel, AgILgel, and Agilegel groups compared with the PBS group, indicating that our AgNCs-based wound dressings were good for infected wound healing. Interestingly, these markers were also significantly increased in the Agilegel group compared with the AgILgel group, suggesting that released VEGF- $\alpha$  could effectively promote proliferation, angiogenesis, and ECM formation after the attenuation of inflammation. IF staining analysis also revealed that the levels of Ki67 (2.1-fold), CD31 (2.7-fold), and  $\alpha$ -SMA (1.7-fold) in the skins of the Agilegel group were higher than those in the AgILgel group (Figure 5B, C). Moreover, WB analysis also showed that the Agilegel treatment significantly increased the protein expression of PCNA (1.6-fold), CD31 (1.5-fold), and  $\alpha$ -SMA (1.6-fold) to the AgILgel group (Figure 5D, E). Taken together, these results demonstrate that Agilegel effectively promotes proliferation, angiogenesis, and ECM formation, thereby accelerating the regeneration of granular tissue.

### CONCLUSION

In conclusion, we have successfully developed Agilegel, a DNA-based and multidrug sequential-release hydrogel, which demonstrates the ability to regulate the release kinetics of VEGF- $\alpha$ , AgNCs, and IL-10 through covalent bonds, non-covalent bonds, and physical encapsulation within its hierarchical structures. This special feature enables the controlled release of VEGF- $\alpha$ , AgNCs, and IL-10 at different stages of wound healing, allowing each component to fulfill its specific role. Agilegel has shown remarkable therapeutic potential in the treatment of diabetic wounds. It effectively eradicates bacterial infection, scavenges ROS, promotes macrophage polarization from pro-inflammatory M1 to anti-inflammatory M2 phenotype, and accelerates cell proliferation, angiogenesis, and ECM formation. Eventually, Agilegel accelerates the closure of DWs. Compared with other versatile hydrogels, Agilegel's hierarchical structure gives it the ability to precisely modulate the dynamics of drug release. This capability is essential to manage the phased intervention of multiple drugs in the treatment of complex wounds.

Hydrogels hold great promise for multiple drug delivery in the treatment of complex wounds and other challenging diseases. In order to achieve accurate control of the release dynamics of different drugs at different stages, it is essential to fully exploit the structural properties of nanomaterials and leverage their chemical or physical interactions at drug loading sites. Our study provides a promising strategy for the integration and sequential release of multiple drugs. A programmable DNA molecule can endow its microscopic or

macroscopic structure with predetermined drug loading sites, providing an influential avenue for phased interventions in the treatment of complex wounds and other multifaceted diseases.

## EXPERIMENTAL SECTION

### Materials

All DNA oligonucleotide strands were purchased from the BBI Life Sciences Corporation. NHS-Alexa647 and NHS-Alexa488 were purchased from Thermo Fisher Scientific. Recombinant mouse IL-10 was purchased from Novoprotein Scientific Inc. VEGF- $\alpha$  was purchased from Chamot Biotechnology Co., Ltd. and streptozotocin (STZ) was purchased from Sigma-Aldrich. Pentobarbital was obtained from Merck. All other chemicals or materials were purchased from Sigma-Aldrich and used as received unless otherwise stated.

### Design and Synthesis of Antibacterial AgNCs-Y Nanostructure

DNA-templated AgNCs were synthesized and stabilized in an aqueous solution by DNA scaffolds with six-base cytosine loops ( $C_6$  loop). Three ssDNA strands (Y1/Y2/Y3) were designed (Table S1) and annealed to assemble into Y-shaped DNA nanostructures. Briefly, all ssDNA was dissolved in 1× PBS (2 mM  $MgCl_2$ , pH = 7.2) with a final concentration of 1 mM. Then 250  $\mu M$  Y1/Y2/Y3 was mixed, respectively, and annealed from 95 to 4 °C to self-assemble into Y monomers. Next,  $AgNO_3$  was added into the Y solutions and reduced by  $NaBH_4$  (molar ratio, Y:  $AgNO_3$ :  $NaBH_4$  = 1:18:18), resulting in the formation of AgNCs-Y.

### Biotin-VEGF- $\alpha$ Modification

Power VEGF- $\alpha$  powder was dissolved in 1× PBS with a final concentration of 100  $\mu g/100 \mu L$ . The biotinylation kit (Abcam, cat. 201795) was used to modify VEGF- $\alpha$  according to the protocol provided by the manufacturer.

### Conjugation of Biotin-VEGF- $\alpha$ with L Monomer

In order to conjugate biotin-VEGF- $\alpha$  with the L monomer, ssDNA L4 was modified with biotin (biotin-L4). Here, a 375  $\mu M$  amount of biotin-L4 and L5 was mixed in 1 × PBS (2 mM  $MgCl_2$ , pH = 7.2) and annealed from 95 to 4 °C to self-assemble into the cross-linker structure monomer (biotin-L). And then, 2  $\mu L$  of 2.5 mg/mL (33  $\mu M$ ) of streptavidin (SA) was mixed with 100  $\mu L$  of 375  $\mu M$  of biotin-L structure for 1 h. After that, 0.94  $\mu L$  of 800 ng/ $\mu L$  biotin-VEGF- $\alpha$  was added into the mixture for 1 h, and VEGF- $\alpha$ -L structure could be obtained.

### Synthesis of Agilegel

An volume of 102  $\mu L$  of the 364  $\mu M$  L/VEGF- $\alpha$ -L (containing 750 ng VEGF- $\alpha$ ) sample was first incubated with 5  $\mu L$  of 1  $\mu g/\mu L$  IL-10 and then mixed with 45  $\mu L$  of 38.3  $\mu g/mL$  (450  $\mu M$  AgNCs) AgNCs-Y, 98  $\mu L$  of 250  $\mu M$  Y structure to assemble into Agilegel at 25–28 °C. The solution state of the mixture transformed into the gel state within 1–2 min.

### Rheological Analysis of Agilegel

The ARES-RFS rheometer (ARES-G2) with 8 mm parallel-plate geometry was used to conduct rheological tests. Viscosity curves were recorded during rotational runs at 25 °C. In addition, a time-scan test was carried out at a fixed strain of 1% and frequency of 1 Hz at 25 °C.

### Release Kinetics of Different Dyes

Here, we used fluorescent dyes to represent the cargo since the fluorescent signal of released AgNCs was difficult to detect. Three different dyes were integrated into DNA hydrogel, where Cy3 was covalently conjugated to L-shaped DNA monomer (conjugated dye), STYO 60 was embedded in the DNA backbone (embedded dye), and Alexa488 was encapsulated within the holes of DNA hydrogel (encapsulated dye). A volume of 200  $\mu L$  of DNA hydrogel was placed at the bottom of the 1.5 mL EP tube, followed by the addition of 200  $\mu L$  of 1× PBS, and the EP tube was placed flat at 37 °C. The supernatants were collected from the EP tube and replaced daily with

fresh PBS. The fluorescent dyes in the collected supernatants were measured using a fluorescence spectrometer.

### Modification of Biotin-VEGF- $\alpha$ and IL-10 with Fluorophores

Here, 10  $\mu L$  of 100  $\mu g/100 \mu L$  biotin-VEGF- $\alpha$  was mixed with 1  $\mu L$  of 10 mM NHS-Alexa647 in PBS (pH = 8) for 2 h. Then 10  $\mu L$  of 100  $\mu g/100 \mu L$  IL-10 was mixed with 1  $\mu L$  of 10 mM NHS-Alexa488 in PBS (pH = 8) for 2 h. Both excess NHS-Alexa647 and excess NHS-Alexa488 were removed by Zeba spin desalting columns (7 K MWCO, 0.5 mL, Thermo Scientific, cat. 89882).

### Cell Culture

Human epidermal keratinocyte (HaCaT) cell lines were cultured in Dulbecco's modified Eagle's medium (DMEM, Gibco) and supplemented with 100 IU/mL penicillin, 100  $\mu g/mL$  streptomycin, and 10% FBS (Inner Mongolia Opcel Biotechnology Co., Ltd.) at 37 °C in a humidified 5%  $CO_2$  incubator.

### ROS Scavenging In Vitro

•OH was produced by the Fenton reaction, where  $H_2O_2$  (3 mM) and  $FeCl_2$  (1 mM) were mixed in ultrapure water (18  $M\Omega$  cm) at room temperature for 30 min and then incubated with water (control group), the Y-DNA monomer (50  $\mu M$ ), AgNCs-Y (50  $\mu M$ ) and the L-DNA monomer (50  $\mu M$ ) in ultrapure water for 30 min respectively. After that, the •OH probe methylenebenzidine (MB, 30  $\mu M$ ) was added into each group and incubated for 2 h. The •OH-scavenging ability was quantified by measuring the absorbance of MB at 666 nm. The absorbance of MB in the MB group was named  $MB_0$ , in the control group named  $MB_f$ , and in the other groups named  $MB_{measure}$ ; therefore, •OH-scavenging efficiency was calculated by the following formula:

$$\left( 1 - \frac{MB_0 - MB_{measure}}{MB_0 - MB_f} \right) \times 100\%$$

### Intracellular ROS-Scavenging Property of DNA Monomers

HaCaT cells were incubated overnight with 500  $\mu M$   $H_2O_2$  to produce intracellular ROS, followed by incubation with the Y DNA monomer (50  $\mu M$ ), AgNCs-Y (50  $\mu M$ ), and the L DNA monomer (50  $\mu M$ ). Cells were then stained with ROS probe DCFH-DA (10  $\mu M$ , Molecular Probes, Invitrogen) for 20 min at 37 °C, and imaged with fluorescence microscopy (Leica, THUNDER Imager DMI8, Germany).

### Ethical Statement

All animal experiments were approved by the Animal Care and Use Committee of West China Hospital, Sichuan University (No.20220118002).

### In Vivo Optical Imaging of the Release-Retention of IL-10 and VEGF- $\alpha$

Adult male C57BL/6 mice (23–25 g) were purchased from Ensiweiwei Experimental Animals Co. (Chengdu, China). The diabetic model was induced by intraperitoneal injection of STZ (180 mg/kg). On days 9 and 10, nonfasting blood glucose (NFBG) was measured and mice with NFBG above 16.7 mM were used to induce a diabetic wound model. The 0.8 cm full-thickness skin wound model was made as previously described.<sup>27</sup> IL-10 and VEGF- $\alpha$  were labeled with Alexa488 and Alexa647 respectively. We injected Agilegel (150 ng of Alexa647-VEGF- $\alpha$  and 1  $\mu g$  of Alexa488-IL-10 in 50  $\mu L$  Agilegel) locally into the wound beds after wound induction and monitored the fluorescence signal of IL-10 and VEGF- $\alpha$  at day 0, 2, 4, 6, 8, and 10 on a Multi-Model In Vivo Animal Imaging System (AniView100, Guangzhou Biolight Biotechnology, Guangzhou, China). The mixture of free IL-10 and free VEGF- $\alpha$  was used as the control.

### Bacteria Culture

Gram-positive *Staphylococcus aureus* (*S. aureus*) and Gram-negative *Escherichia coli* (*E. coli*) were employed in the experiment. Bacterial cells were prepared by inoculating a single bacterial colony from a

Luria–Bertani (LB) plate and then suspended in 3 mL LB medium at 37 °C and shaken at 200 rpm for 12 h. The number of bacteria was estimated by measuring the absorbance of the medium at 600 nm using a UV–vis spectrophotometer.

### **In Vitro Antibacterial Experiments**

The antibacterial activity of AgNCs-Y was determined by an agar plate dilution method. First, the bacterial strains *S. aureus* or *E. coli* ( $10^7$  CFU mL<sup>-1</sup>) were cultured with AgNCs-Y at different concentrations (0, 1.7, 3.4, and 6.8 μg/mL) in PBS at 37 °C under shaking at 220 rpm for 4 h. Next, the bacterial suspension was diluted in appropriate folds in LB, and 100 μL of the bacterial diluent (*S. aureus* and *E. coli*) was applied to the LB agar plate. Finally, the agar plates were cultured at 37 °C for different times (12 h for *S. aureus* and 24 h for *E. coli*) and counted statistically. Each group of three was run in parallel.

### **Live/Dead Bacteria Assay**

The antibacterial activity of AgNCs-Y was evaluated by using visualized fluorescence imaging. The viability of bacterial cells was determined using SYTO9 and PI dye (Invitrogen Detection Technologies, USA). SYTO9 with green fluorescence stain both dead and live bacteria, whereas PI with red fluorescence stain only dead bacteria. Briefly, cells were treated with AgNCs-Y for 4 h at 37 °C. Next, the bacterial cells were washed with PBS and incubated with PI and SYTO9 dye for 20 min at 37 °C in the dark. Finally, the cells were imaged using confocal laser scanning microscopy (Leica TCS SP8, Germany).

### **Antibacterial Activity Assay In Vivo**

The antibacterial activity of the AgNCgel was evaluated by using the plant count method *in vivo*. After induction of the diabetic wound, all mice were inoculated with freshly  $5 \times 10^6$  CFU *S. aureus* (50 μL) in wound beds. On days 1 and 3, the wounds were washed with 100 μL of PBS three times. And the suspension was diluted with PBS, followed by being plated onto LB agar plates and incubated at 37 °C for 12 h. Digital images of the bacterial colonies were taken. The number of bacterial colonies was counted.

### **Wound Healing In Vivo**

After diabetic wound induction, all mice were inoculated with fresh  $5 \times 10^6$  CFU *S. aureus* (50 μL) into the wound beds. Diabetic mice with infected wounds were randomly treated with PBS (50 μL, PBS,  $n = 12$ ), IL-10 (IL-10, 1 μg in 50 μL PBS,  $n = 6$ ), AgNCgel (50 μL,  $n = 12$ ), AgILgel (1 μg of IL-10 in 50 μL AgILgel,  $n = 12$ ), and Agilegel (150 ng of VEGF- $\alpha$  and 1 μg of IL-10 in 50 μL Agilegel,  $n = 6$ ). Wounds were photographed on days 0, 3, 7, and 12 after surgery and the wound area was measured and analyzed by tracing the wound borders using ImageJ software.

The mice in each group were sacrificed at day 3 ( $n = 6$  from PBS, IL-10, AgNCgel, and AgILgel groups) and day 12 ( $n = 6$  from PBS, AgNCgel, AgILgel, and Agilegel groups) postwound. Wound skin samples were collected for further tests.

### **Mitochondrial ROS (mtROS) Assay**

mtROS of skin tissue was measured using mitochondrial superoxide indicators according to the manufacturer's instructions. The stained slices were observed by fluorescence microscopy (Thunder Imager DMI8).

### **Quantitative Real-Time Polymerase Chain Reaction (qRT-PCR)**

Total RNA from skin tissues was isolated according to the manufacturer's instructions (MitoSOX, Yeasen, 40778ES50). RNA was quantified and reverse transcribed to cDNA. Primer sequences are listed in Table S2. The qRT-PCR analysis was performed on a CFX96 Real-Time PCR Detection System (Bio-Rad) with an SYBR green supermix.

### **Western Blotting Analysis**

The total proteins of the skin tissue were extracted and quantified with a BCA protein assay kit (KeyGEN BioTECH). Equal amounts of

protein were subjected to electrophoresis on 10% SDS-PAGE, transferred to PVDF membranes. After that, the membranes were blocking in 5% nonfat skim milk with TBST for 1 h followed by incubated with primary antibodies including anti-iNOS (ab202417, 1:1000, Abcam), anti-mannose receptor (CD206, ab300621, 1:1000, Abcam), anti-PCNA (ab92552, 1:1000, Abcam), anti-CD31 (ab222783, 1:1000, Abcam), anti- $\alpha$ -SMA (S5135-1-AP, 1:1000, Proteintech), and anti-GAPDH (1:10000, Huabio, Hangzhou, China) at 4 °C overnight. Then the membranes were washed 3 times and incubated with secondary antibodies (ZSGB-Bio, Beijing, China) for 1 h at 37 °C. Last, the proteins were visualized using ECL substrate (Bio-Rad) and analyzed with ImageJ software.

### **Histological Staining**

Skin tissue was fixed, embedded in paraffin, and sliced for HE and IF staining. For IF staining, sections were first blocking in 1% BSA for 1 h, and then incubated overnight with diluted primary antibodies including rat anti-mouse F4/80 (Arigo), rabbit anti-mouse iNOS, rabbit anti-mouse CD206, rabbit anti-Ki67, anti-CD31, and anti-Alpha-smooth muscle actin ( $\alpha$ -SMA) (all from Abcam, USA), followed by fluorescence-conjugated secondary antibody staining for 1 h. Images of the stained sections were acquired by a microscope (Carl Zeiss, Germany), and quantitative analysis of the histological images was measured by ImageJ software.

### **Statistical Analysis**

All quantitative data are presented as mean  $\pm$  SEM. GraphPad software was used to do the statistical analyses. Student's *t* test was employed for comparisons between the two groups. One-way analysis of variance (ANOVA) followed by Tukey's ad hoc test was used for multiple comparisons. A *P*-value less than 0.05 was considered statistically significant. \**P* < 0.05, \*\**P* < 0.01, \*\*\**P* < 0.001, \*\*\*\**P* < 0.0001. #*P* < 0.05, ##*P* < 0.01, ###*P* < 0.001, ####*P* < 0.0001.

## ■ ASSOCIATED CONTENT

### SI Supporting Information

The Supporting Information is available free of charge at <https://pubs.acs.org/doi/10.1021/jacsau.3c00408>.

Simulated structure of the Y monomer; PAGE characterization of ssDNA and Y monomer; fluorescent AGE characterization of AgNCs-Y; retention of free IL-10 and VEGF- $\alpha$  *in vivo*; representative SEM image of *S. aureus* and *E. coli* treated with PBS and AgNCs-Y; cytotoxicity of different concentrations of AgNCs-Y and cell viability analysis by CCK-8 assay; biodegradation process of Agilegel monitored by *in vivo* imaging system; ROS scavenging ability of DNA; sequence of single-stranded oligonucleotides used for the synthesis of the Y and L monomers; primers used for qPCR analysis (PDF)

## ■ AUTHOR INFORMATION

### Corresponding Authors

**Ying Zhu** – Institute of Materiobiology, Department of Chemistry, College of Science, Shanghai University, Shanghai 200444, China; The Interdisciplinary Research Center, Shanghai Synchrotron Radiation Facility, Shanghai Advanced Research Institute, Chinese Academy of Sciences, Shanghai 201210, China; Email: [zhuying@sinap.ac.cn](mailto:zhuying@sinap.ac.cn)

**Chengshi Wang** – Department of Endocrinology and Metabolism, Center for Diabetes and Metabolism Research, West China Hospital, Sichuan University, Chengdu 610041, China; Email: [wangchengshi@wchscu.cn](mailto:wangchengshi@wchscu.cn)

**Min Lv** – College of Chemistry and Materials Science, Shanghai Normal University, Shanghai 200234, China;

orcid.org/0000-0003-0587-8528; Email: lvmin@shnu.edu.cn

## Authors

**Wei Li** – Department of Endocrinology and Metabolism, Center for Diabetes and Metabolism Research, West China Hospital, Sichuan University, Chengdu 610041, China

**Hui Xie** – College of Chemistry and Materials Science, Shanghai Normal University, Shanghai 200234, China

**Liping Gou** – Department of Endocrinology and Metabolism, Center for Diabetes and Metabolism Research, West China Hospital, Sichuan University, Chengdu 610041, China

**Ye Zhou** – Department of Endocrinology and Metabolism, Center for Diabetes and Metabolism Research, West China Hospital, Sichuan University, Chengdu 610041, China

**Hao Wang** – Laboratory of Dermatology, West China Hospital, Sichuan University, Chengdu 610041, China

**Ruoqing Li** – Department of Endocrinology and Metabolism, Center for Diabetes and Metabolism Research, West China Hospital, Sichuan University, Chengdu 610041, China; Department of General Medicine, Chongqing University Central Hospital, Chongqing Emergency Medical Center, Chongqing Key Laboratory of Emergency Medicine, Chongqing 400014, China

**Yong Zhang** – Key Laboratory of Transplant Engineering and Immunology, West China Hospital, Sichuan University, Chengdu 610041, China; orcid.org/0000-0003-0513-8941

**Shuyun Liu** – Key Laboratory of Transplant Engineering and Immunology, West China Hospital, Sichuan University, Chengdu 610041, China

**Jingping Liu** – Key Laboratory of Transplant Engineering and Immunology, West China Hospital, Sichuan University, Chengdu 610041, China; orcid.org/0000-0001-8364-639X

**Yanrong Lu** – Key Laboratory of Transplant Engineering and Immunology, West China Hospital, Sichuan University, Chengdu 610041, China

**Zhengliang Eric He** – Shanghai Soong Ching Ling School, Shanghai 201703, China

**Nan Chen** – College of Chemistry and Materials Science, Shanghai Normal University, Shanghai 200234, China; orcid.org/0000-0001-8536-6631

**Jiang Li** – Institute of Materiobiology, Department of Chemistry, College of Science, Shanghai University, Shanghai 200444, China; The Interdisciplinary Research Center, Shanghai Synchrotron Radiation Facility, Shanghai Advanced Research Institute, Chinese Academy of Sciences, Shanghai 201210, China

Complete contact information is available at: <https://pubs.acs.org/10.1021/jacsau.3c00408>

## Author Contributions

<sup>¶</sup>W.L. and H.X. contributed equally to this work. W.L. and M.L. conceived the project and wrote the manuscript. W.L., H.X., and C.W. performed the experiments and analyzed the data. L.G., Y.Z., H.W., R.L., Y.Z., S.L., J.L., Y.L., and Z.E.H. analyzed the data and participated in discussions. N.C., Chunhai Fan, J.L., and Y.Z. revised the manuscript.

## Notes

The authors declare no competing financial interest.

## ACKNOWLEDGMENTS

This work was financially supported by the National Key R&D Program of China (2020YFA0908900), the National Natural Science Foundation of China (31971310, 22022410, 82050005), the China Postdoctoral Science Foundation (2021TQ0225, 2021M702370), the Post-Doctor Research Project, West China Hospital of Sichuan University (2021HXBH065), Program of Natural Science Foundation of Sichuan (2022NSFSC1559, 2022NSFSC1569), 2022 Shanghai “Science and Technology Innovation Action Plan” Fundamental Research Project (22JC1401203) and the Youth Innovation Promotion Association CAS (2016236), the Sichuan University Postdoctoral Interdisciplinary Innovation Fund, Chongqing Key Laboratory of Emergency Medicine (2022KFKT03).

## REFERENCES

- (1) Falanga, V. Wound healing and its impairment in the diabetic foot. *Lancet* **2005**, *366* (9498), 1736–1743.
- (2) Gurtner, G. C.; Werner, S.; Barrandon, Y.; Longaker, M. T. Wound repair and regeneration. *Nature* **2008**, *453* (7193), 314–321.
- (3) Tu, C.; Lu, H.; Zhou, T.; Zhang, W.; Deng, L.; Cao, W.; Yang, Z.; Wang, Z.; Wu, X.; Ding, J.; Xu, F.; Gao, C. Promoting the healing of infected diabetic wound by an anti-bacterial and nano-enzyme-containing hydrogel with inflammation-suppressing, ROS-scavenging, oxygen and nitric oxide-generating properties. *Biomaterials* **2022**, *286*, No. 121597.
- (4) Kharaziha, M.; Baidya, A.; Annabi, N. Rational Design of Immunomodulatory Hydrogels for Chronic Wound Healing. *Adv. Mater.* **2021**, *33* (39), No. e2100176.
- (5) Boulton, A. J.; Vileikyte, L.; Ragnarson-Tennvall, G.; Apelqvist, J. The global burden of diabetic foot disease. *Lancet* **2005**, *366* (9498), 1719–1724.
- (6) Zhao, H.; Huang, J.; Li, Y.; Lv, X.; Zhou, H.; Wang, H.; Xu, Y.; Wang, C.; Wang, J.; Liu, Z. ROS-scavenging hydrogel to promote healing of bacteria infected diabetic wounds. *Biomaterials* **2020**, *258*, No. 120286.
- (7) Al Sadoun, H. Macrophage Phenotypes in Normal and Diabetic Wound Healing and Therapeutic Interventions. *Cells* **2022**, *11* (15), 2430.
- (8) Zhao, R.; Liang, H.; Clarke, E.; Jackson, C.; Xue, M. Inflammation in Chronic Wounds. *Int. J. Mol. Sci.* **2016**, *17* (12), 2085.
- (9) Dunnill, C.; Patton, T.; Brennan, J.; Barrett, J.; Dryden, M.; Cooke, J.; Leaper, D.; Georgopoulos, N. T. Reactive oxygen species (ROS) and wound healing: the functional role of ROS and emerging ROS-modulating technologies for augmentation of the healing process. *Int. Wound J.* **2017**, *14* (1), 89–96.
- (10) Frykberg, R. G.; Banks, J. Challenges in the Treatment of Chronic Wounds. *Adv. Wound Care* **2015**, *4* (9), 560–582.
- (11) Huang, K.; Liu, W.; Wei, W.; Zhao, Y.; Zhuang, P.; Wang, X.; Wang, Y.; Hu, Y.; Dai, H. Photothermal Hydrogel Encapsulating Intelligently Bacteria-Capturing Bio-MOF for Infectious Wound Healing. *ACS Nano* **2022**, *16* (11), 19491–19508.
- (12) Liang, Y.; Li, M.; Yang, Y.; Qiao, L.; Xu, H.; Guo, B. pH/Glucose Dual Responsive Metformin Release Hydrogel Dressings with Adhesion and Self-Healing via Dual-Dynamic Bonding for Athletic Diabetic Foot Wound Healing. *ACS Nano* **2022**, *16* (2), 3194–3207.
- (13) Xiong, Y.; Chen, L.; Liu, P.; Yu, T.; Lin, C.; Yan, C.; Hu, Y.; Zhou, W.; Sun, Y.; Panayi, A. C.; Cao, F.; Xue, H.; Hu, L.; Lin, Z.; Xie, X.; Xiao, X.; Feng, Q.; Mi, B.; Liu, G. All-in-One: Multifunctional Hydrogel Accelerates Oxidative Diabetic Wound Healing through Timed-Release of Exosome and Fibroblast Growth Factor. *Small* **2022**, *18* (1), No. e2104229.
- (14) Wu, H.; Li, F.; Shao, W.; Gao, J.; Ling, D. Promoting Angiogenesis in Oxidative Diabetic Wound Microenvironment Using

- a Nanozyme-Reinforced Self-Protecting Hydrogel. *ACS Cent. Sci.* **2019**, *5* (3), 477–485.
- (15) Wang, S.; Zheng, H.; Zhou, L.; Cheng, F.; Liu, Z.; Zhang, H.; Wang, L.; Zhang, Q. Nanoenzyme-Reinforced Injectable Hydrogel for Healing Diabetic Wounds Infected with Multidrug Resistant Bacteria. *Nano Lett.* **2020**, *20* (7), 5149–5158.
- (16) Xing, Y.; Cheng, E.; Yang, Y.; Chen, P.; Zhang, T.; Sun, Y.; Yang, Z.; Liu, D. Self-assembled DNA hydrogels with designable thermal and enzymatic responsiveness. *Adv. Mater.* **2011**, *23* (9), 1117–1121.
- (17) Dong, Y.; Yao, C.; Zhu, Y.; Yang, L.; Luo, D.; Yang, D. DNA Functional Materials Assembled from Branched DNA: Design, Synthesis, and Applications. *Chem. Rev.* **2020**, *120* (17), 9420–9481.
- (18) Li, J.; Zheng, C.; Cansiz, S.; Wu, C.; Xu, J.; Cui, C.; Liu, Y.; Hou, W.; Wang, Y.; Zhang, L.; Teng, I. T.; Yang, H. H.; Tan, W. Self-assembly of DNA nanohydrogels with controllable size and stimuli-responsive property for targeted gene regulation therapy. *J. Am. Chem. Soc.* **2015**, *137* (4), 1412–1415.
- (19) Ren, N.; Sun, R.; Xia, K.; Zhang, Q.; Li, W.; Wang, F.; Zhang, X.; Ge, Z.; Wang, L.; Fan, C.; Zhu, Y. DNA-Based Hybrid Hydrogels Sustain Water-Insoluble Ophthalmic Therapeutic Delivery against Allergic Conjunctivitis. *ACS Appl. Mater. Interfaces* **2019**, *11* (30), 26704–26710.
- (20) Mo, F.; Jiang, K.; Zhao, D.; Wang, Y.; Song, J.; Tan, W. DNA hydrogel-based gene editing and drug delivery systems. *Adv. Drug Delivery Rev.* **2021**, *168*, 79–98.
- (21) Yuan, T.; Shao, Y.; Zhou, X.; Liu, Q.; Zhu, Z.; Zhou, B.; Dong, Y.; Stephanopoulos, N.; Gui, S.; Yan, H.; Liu, D. Highly Permeable DNA Supramolecular Hydrogel Promotes Neurogenesis and Functional Recovery after Completely Transected Spinal Cord Injury. *Adv. Mater.* **2021**, *33* (35), No. e2102428.
- (22) Xiong, Z.; Sun, L.; Yang, H.; Xiao, Z.; Deng, Z.; Li, Q.; Wang, C.; Shen, F.; Liu, Z. Ni-Alginate Hydrogel Microspheres with Sustained Interleukin 2 Release to Boost Cytokine-Based Cancer Immunotherapy. *Adv. Funct. Mater.* **2023**, *33* (7), No. 2211423.
- (23) Zhang, J.; Guo, Y.; Pan, G.; Wang, P.; Li, Y.; Zhu, X.; Zhang, C. Injectable Drug-Conjugated DNA Hydrogel for Local Chemotherapy to Prevent Tumor Recurrence. *ACS Appl. Mater. Interfaces* **2020**, *12* (19), 21441–21449.
- (24) Yan, X.; Yang, B.; Chen, Y.; Song, Y.; Ye, J.; Pan, Y.; Zhou, B.; Wang, Y.; Mao, F.; Dong, Y.; Liu, D.; Yu, J. Anti-Friction MSCs Delivery System Improves the Therapy for Severe Osteoarthritis. *Adv. Mater.* **2021**, *33* (52), No. e2104758.
- (25) Zhang, C.; Huang, H.; Chen, J.; Zuo, T.; Ou, Q.; Ruan, G.; He, J.; Ding, C. DNA Supramolecular Hydrogel-Enabled Sustained Delivery of Metformin for Relieving Osteoarthritis. *ACS Appl. Mater. Interfaces* **2023**, *15* (13), 16369–16379.
- (26) Li, W.; Wang, C.; Wang, Z.; Gou, L.; Zhou, Y.; Peng, G.; Zhu, M.; Zhang, J.; Li, R.; Ni, H.; Wu, L.; Zhang, W.; Liu, J.; Tian, Y.; Chen, Z.; Han, Y.-P.; Tong, N.; Fu, X.; Zheng, X.; Berggren, P.-O. Physically Cross-Linked DNA Hydrogel-Based Sustained Cytokine Delivery for In Situ Diabetic Alveolar Bone Rebuilding. *ACS Appl. Mater. Interfaces* **2022**, *14* (22), 25173–25182.
- (27) Wang, Z.; Li, W.; Gou, L.; Zhou, Y.; Peng, G.; Zhang, J.; Liu, J.; Li, R.; Ni, H.; Zhang, W.; Cao, T.; Cao, Q.; Su, H.; Han, Y. P.; Tong, N.; Fu, X.; Ilegems, E.; Lu, Y.; Berggren, P. O.; Zheng, X.; Wang, C. Biodegradable and Antioxidant DNA Hydrogel as a Cytokine Delivery System for Diabetic Wound Healing. *Adv. Healthc. Mater.* **2022**, *11* (21), No. e2200782.
- (28) Balasubramanian, B.; Pogozelski, W. K.; Tullius, T. D. DNA strand breaking by the hydroxyl radical is governed by the accessible surface areas of the hydrogen atoms of the DNA backbone. *Proc. Natl. Acad. Sci. U. S. A.* **1998**, *95* (17), 9738–9743.
- (29) Zhao, J.; Guo, Y.; Tong, Z.; Zhang, R.; Yao, C.; Yang, D. Spatio-Temporal Controlled Gene-Chemo Drug Delivery in a DNA Nanocomplex to Overcome Multidrug Resistance of Cancer Cells. *ACS Appl. Bio Mater.* **2022**, *5* (8), 3795–3805.
- (30) Liu, J.; Song, L.; Liu, S.; Zhao, S.; Jiang, Q.; Ding, B. A Tailored DNA Nanopatform for Synergistic RNAi-/Chemotherapy of Multi-drug-Resistant Tumors. *Angew. Chem., Int. Ed. Engl.* **2018**, *57* (47), 15486–15490.
- (31) Song, L.; Xiao, M.; Lai, W.; Li, L.; Wan, Y.; Pei, H. Intracellular Logic Computation with Framework Nucleic Acid-Based Circuits for mRNA Imaging. *Chin. J. Chem.* **2021**, *39* (4), 947–953.
- (32) Javani, S.; Lorca, R.; Latorre, A.; Flors, C.; Cortajarena, A. L.; Somoza, Á. Antibacterial Activity of DNA-Stabilized Silver Nanoclusters Tuned by Oligonucleotide Sequence. *ACS Appl. Mater. Interfaces* **2016**, *8* (16), 10147–10154.
- (33) Wu, J.; Li, F.; Hu, X.; Lu, J.; Sun, X.; Gao, J.; Ling, D. Responsive Assembly of Silver Nanoclusters with a Biofilm Locally Amplified Bactericidal Effect to Enhance Treatments against Multi-Drug-Resistant Bacterial Infections. *ACS Cent. Sci.* **2019**, *5* (8), 1366–1376.
- (34) Liu, S.; Yan, Q.; Cao, S.; Wang, L.; Luo, S.-H.; Lv, M. Inhibition of Bacteria *In Vitro* and *In Vivo* by Self-Assembled DNA-Silver Nanocluster Structures. *ACS Appl. Mater. Interfaces* **2022**, *14* (37), 41809–41818.
- (35) Zheng, K.; Setyawati, M. I.; Lim, T.-P.; Leong, D. T.; Xie, J. Antimicrobial Cluster Bombs: Silver Nanoclusters Packed with Daptomycin. *ACS Nano* **2016**, *10* (8), 7934–7942.
- (36) Yang, L.; Yao, C.; Li, F.; Dong, Y.; Zhang, Z.; Yang, D. Synthesis of Branched DNA Scaffolded Super-Nanoclusters with Enhanced Antibacterial Performance. *Small* **2018**, *14* (16), No. e1800185.
- (37) Ouyang, W.; O'Garra, A. IL-10 Family Cytokines IL-10 and IL-22: from Basic Science to Clinical Translation. *Immunity* **2019**, *50* (4), 871–891.
- (38) Tang, T. T.; Wang, B.; Wu, M.; Li, Z. L.; Feng, Y.; Cao, J. Y.; Yin, D.; Liu, H.; Tang, R. N.; Crowley, S. D.; Lv, L. L.; Liu, B. C. Extracellular vesicle-encapsulated IL-10 as novel nanotherapeutics against ischemic AKI. *Sci. Adv.* **2020**, *6* (33), No. eaaz0748.
- (39) Nagata, K.; Nishiyama, C. IL-10 in Mast Cell-Mediated Immune Responses: Anti-Inflammatory and Proinflammatory Roles. *Int. J. Mol. Sci.* **2021**, *22* (9), 4972.
- (40) Nissen, N. N.; Polverini, P. J.; Koch, A. E.; Volin, M. V.; Gamelli, R. L.; DiPietro, L. A. Vascular endothelial growth factor mediates angiogenic activity during the proliferative phase of wound healing. *Am. J. Pathol.* **1998**, *152* (6), 1445–1452.
- (41) Guo, R.; Xu, S.; Ma, L.; Huang, A.; Gao, C. The healing of full-thickness burns treated by using plasmid DNA encoding VEGF-165 activated collagen-chitosan dermal equivalents. *Biomaterials* **2011**, *32* (4), 1019–1031.
- (42) Guo, W.; Orbach, R.; Mironi-Harpaz, I.; Seliktar, D.; Willner, I. Fluorescent DNA hydrogels composed of nucleic acid-stabilized silver nanoclusters. *Small* **2013**, *9* (22), 3748–3752.
- (43) Chen, Q.; Ding, F.; Zhang, S.; Li, Q.; Liu, X.; Song, H.; Zuo, X.; Fan, C.; Mou, S.; Ge, Z. Sequential Therapy of Acute Kidney Injury with a DNA Nanodevice. *Nano Lett.* **2021**, *21* (10), 4394–4402.
- (44) Jiang, D.; Ge, Z.; Im, H. J.; England, C. G.; Ni, D.; Hou, J.; Zhang, L.; Kuttyreff, C. J.; Yan, Y.; Liu, Y.; et al. DNA origami nanostructures can exhibit preferential renal uptake and alleviate acute kidney injury. *Nat. Biomed. Eng.* **2018**, *2* (11), 865–877.